

# Electronic and Molecular Structure of Carbazole Using Spectrophotometric and *In Silico* Methods

Andrews Quashie\*

University of Cape Coast, Cape Coast, Ghana

\*Corresponding author: Andrews Quashie, University of Cape Coast, Cape Coast, Ghana, Tel: 233207500120, E-mail: andrews\_q@yahoo.com; andy.quash@gmail.com

Citation: Andrews Quashie (2018) Electronic and Molecular Structure of Carbazole Using Spectrophotometric and *In Silico* Methods. J Nanosci Nanotechnol Appl 2: 106

Article history: Received: 12 February 2018, Accepted: 27 March 2018, Published: 28 March 2018

## Abstract

Carbazole has extensive potential application in supramolecular chemistry and pharmaceutical chemistry due to its rigid structure and large  $\pi$  conjugated system. The electronic structure and molecular orbital data of Carbazole were studied using spectroscopic methods and computational analyses were used to explain some of the properties and to predict others. In this study, calculated structural parameters with the Density Functional Theory at the B3LYP level of theory using 3-21G basis set gave a better approximation to the experimentally determined parameters than the 6-31Gd basis set. The Dunning correlation consistent basis set, cc-pVDZ, gave a better fit than the LanL2DZ basis set of the calculated UV spectrum to the experimentally determined UV spectrum. The reduction of the band gap when Carbazole is dissolved in a mixed solvent system of Ethanol: Water (1:1) by 6% points to one possible way of manipulating the photoelectrical properties of the molecule.

**Keywords:** Carbazole; Density Functional Theory; VEDA 4; Gaussian 09; Powder X-ray Diffraction

## Introduction

Carbazole and its derivatives are an important type of nitrogen containing heterocyclic compounds that are widespread in nature [1]. The chemistry and biology of Carbazole have attracted an increasing interest over the last 50 years because it possesses desirable electronic and charge transport properties, as well as a large  $\pi$ -conjugated system. This enables various functional groups to be easily introduced into the structurally rigid carbazolyl ring. These characteristics result in the extensive potential application of Carbazole in the field of chemistry (photoelectrical material, dyes, supramolecular recognition) and medicinal chemistry (antitumor, anti-inflammatory, antimicrobial, psychotropic, anti-oxidative) [1-4]. These Carbazole-based compounds are also considered to be potential candidates for electronic applications, such as colour displays, organic semiconductors, lasers and solar cells, as they demonstrate electroactivity and luminescence [5,6].

The molecular and electronic structure of Carbazole is believed to be responsible for all these favourable characteristics of the compound. The electronic and vibrational spectra of Carbazole has been of much interest in the past and a lot of investigations have been done in these areas [7,8]. Lee and Boo used computational methods based on Density Functional Theory (DFT) and *ab initio* methods to calculate the molecular structure and perform normal vibrational mode analyses of Carbazole at the Hartree Fock (HF) and Becke-Lee-Yang-Parr (B3LYP) levels of theory using the 6-31G\* basis set. Their analyses of the vibrational spectra relied on the assumptions that the stronger lines mark the presence of fundamentals. The work by Lee and Boo, though confirming most of the fundamentals published by Bree and Zwarich could not identify some of the modes. They, for example, reported serious disagreement between the value of the fundamental  $\nu_{52}$  from their calculations and that reported by Bree and Zwarich [9,10].

This work uses both *in vitro* (experimental methods) and *in silico* (computational methods) to study the structural and electronic properties of Carbazole. The vibrational spectra were analysed using the Potential Energy Distribution (PED) method which quantitatively describes the contribution to movement of a given group of atoms in a normal mode. The chemical stability of Carbazole was examined using the Frontier Orbital Theory (FOT). The crystal structure of Carbazole was delineated using data reduction of the Powder X-Ray Diffractogram (PXRD).

## Experimentals

### Chemicals

Carbazole was purchased from BDH Chemicals, Poole, England with a minimum assay of 98% and was used without further purification.

A 0.0128M solution of the compound was prepared by dissolving the powder in a mixed solvent system of Ethanol: Water (1:1 by vol.). The solution was used subsequently for the Ultraviolet spectroscopy.

### Infra-Red Spectroscopy

The infra-red spectrum of crystalline Carbazole in the region 4000-400  $\text{cm}^{-1}$  was measured at 4  $\text{cm}^{-1}$  resolution with an average of 23 scans on a Perkin Elmer Spectrum Two FT-IR Spectrophotometer. The spectrum was elaborated using the Spekwin 32 software to convert the transmittance to absorbance [11].

### Ultraviolet Spectroscopy

The UV spectra of carbazole were determined using a Spectroquant Pharo 300 UV-Vis Spectrophotometer in the region 190 nm – 1100 nm. The spectrum was elaborated using the Spekwin 32 software [11].

### Powder X-ray Diffraction

X-ray data was acquired using a PANalytical Empyrean X-ray Diffractometer with a copper anode. The K-alpha1 wavelength was 1.54060Å and the K-alpha2 wavelength was 1.39225Å. The sample of carbazole was scanned continuously in steps of .08 ° in 3 seconds with 2θ from 5.04 ° to 80 ° while spinning. Spekwin 32 software was used to sketch the diffractogram [11].

### Crystal Structure

The crystal structure for carbazole has been determined and published by K. Gajda *et al.* and was visualized using OLEX 2 software and plotted using ORTEP-plot in PLATON version 271014 [12,13](Figure 1).

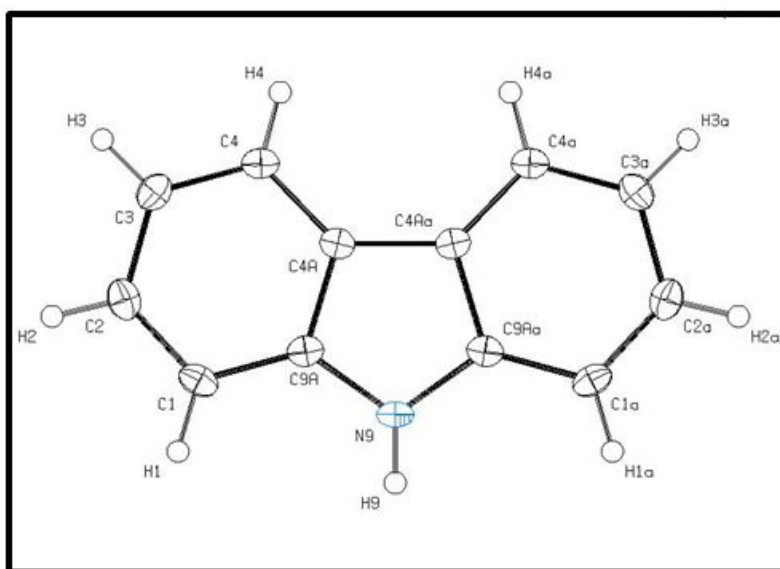


Figure 1: ORTEP plotted and labelled molecule of Carbazole at 50% probability

### Computational Details

The molecular geometry of the compound was optimized using the Gaussian 09 program suite based on the Density Functional Theory (DFT) using the hybrid DFT functional B3LYP and two basis sets; 3-21G, and 6-31Gd basis set [14-33]. For the analysis of the solvent effects on the optimized structure in gas phase, the Continuous Polarizable Continuum Model (CPCM) using Dunning's correlation consistent basis sets, aug-cc-pVDZ (augmented with diffuse functions) and Lanl2DZ were used [34-41].

Frequency calculations at optimized geometry were done to confirm the optimized structures to be at an energy minimum and to obtain the theoretical vibrational spectra. The true energy minimum at the optimized geometry was confirmed by the absence of any imaginary frequency modes.

The Potential Energy Distribution (PED) of the vibrational modes was calculated with the VEDA 4 programme and the vibrational modes were characterized by their total energy distribution (TED%) [42,43].

The possible electronic transitions of the molecules were calculated by finding the energy levels using the TD-SCF DFT method at the B3LYP level of theory. This made possible the visualization of the HOMO and LUMO states.

The natural bond orbital analyses were performed using the NBO calculations as implemented in the Gaussian 09 package.

The percentage contribution of the various groups on the molecule to the various molecular orbitals were confirmed using the GaussSum software based on the Mulliken Population Analysis [44].

## Results and Discussion

### Bond Lengths and Angles

Bond Lengths were measured from both the optimized structure using DFT calculations (referred to as 'calculated') using the two basis sets, 3-21G and 6-31Gd, and the ORTEP-plot of the structure determined by X-ray data refinement of the Single Crystal (SC) structure of the Carbazole molecule as solved by K. Gajda *et al.* and plotted using OLEX 2 and ORTEP-plot in PLATON version 271014 [12].

All calculated bond lengths are longer than determined by SC x-ray data refinement, except Carbon-Carbon bond opposite the nitrogen atom, i.e. C4A-C4Aa using the 6-31Gd basis set. The deviations may be attributed to the crystal packing force (Table 1). This bond is the longest in the pyrrole ring, emphasizing its relative single bond character. This trend is seen in the calculated bond lengths also, though using the 6-31Gd basis set gives a slightly shorter length, 1.4504Å, than the SC x-ray determined length of 1.4534Å (Table 1).

Bond Lengths			
	X-ray	DFT (3-21G)	DFT (6-31Gd)
Bond	Length (Å)		
N9-C9A	1.3844	1.3942	1.3866
C9A-C1	1.3946	1.3957	1.3967
C1-H1	0.9300	1.0836	1.0869
C1-C2	1.3848	1.3940	1.3931
N9-H9	0.8600	1.0112	1.0079
C2-H2	0.9300	1.0838	1.0867
C2-C3	1.4006	1.4063	1.4061
C3-H3	0.9300	1.0834	1.0863
C3-C4	1.3830	1.3938	1.3923
C4-H4	0.9300	1.0840	1.0870
C4-C4A	1.3971	1.3979	1.4001
C4A-C4Aa	1.4534	1.4552	1.4504
C4Aa-C4a	1.3971	1.3979	1.4001
C4a-H4a	0.9300	1.0840	1.0870
C4a-C3a	1.3830	1.3938	1.3923
C3a-H3a	0.9300	1.0834	1.0863
C3a-C2a	1.4006	1.4063	1.4061
C2a-H2a	0.9300	1.0838	1.0867
C2a-C1a	1.3848	1.3940	1.3931
C1a-H1a	0.9300	1.0836	1.0869
C1a-C9Aa	1.3946	1.3957	1.3967
C9Aa-N9	1.3844	1.3942	1.3866
C4A-C9A	1.4145	1.4263	1.4208
C4Aa-C9Aa	1.4145	1.4263	1.4208

**Table 1:** Calculated Bond lengths using DFT compared to Measured Bond lengths from X-ray diffraction data

Additionally, the C - H and N - H bonds calculated were also longer by approximately 0.15Å than those determined from the SC x-ray data refinement. This may be because all hydrogen atoms in the structure refinement of the experimentally determined structure were generated in idealized positions and refined in riding mode [12]. The large deviations from experiment may also arise from the low scattering factors of hydrogen atoms in the X-ray diffraction experiment.

Lengths of C – H bonds in the arene rings and C – C bonds adjacent the pyrrole ring (C1 - C9A and C1a - C9Aa) calculated using the 3-21G basis set were found to deviate less from the experimentally determined ones than when the 6-31Gd basis set was used (Table 1). This is not expected as the 6-31Gd basis is at a higher level of theory. A possible reason is that the polarization effect introduced by the 6-31Gd basis set is not effective.

Bond Angles were also measured from both the optimized structure using DFT calculations (referred to as 'calculated') using the two basis sets, 3-21G and 6-31Gd, and the ORTEP-plot of the structure determined by SC x-ray data refinement (Table 2).

Bond Angles			
	X-ray	DFT (3-21G)	DFT (6-31Gd)
Bond	Angle (°)		
H9-N9-C9A	125.00	125.14	125.16
N9-C9A-C1	129.50	130.36	129.67
C9A-C1-H1	121.00	121.21	121.30
H1-C1-C2	121.00	120.77	121.04
C1-C2-H2	119.00	119.26	119.20
H2-C2-C3	119.00	119.46	119.47
C2-C3-H3	120.00	119.46	119.50
H3-C3-C4	120.00	119.84	119.78
C3-C4-H4	121.00	120.52	120.39
H4-C4-C4A	121.00	120.37	120.39
C4-C4A-C4Aa	133.97	133.61	134.09
C4A-C4Aa-C4a	133.97	133.61	134.09
C4Aa-C4a-H4a	121.00	120.37	120.39
H4a-C4a-C3a	121.00	120.52	120.39
C4a-C3a-H3a	120.00	119.84	119.78
H3a-C3a-C2a	120.00	119.46	119.50
C3a-C2a-H2a	119.00	119.46	119.47
H2a-C2a-C1a	119.00	119.26	119.20
C2a-C1a-H1a	121.00	120.77	121.04
H1a-C1a-C9Aa	121.00	121.21	121.30
C1a-C9Aa-N9	129.50	130.36	129.67
C9Aa-N9-C9A	109.53	109.73	109.69
N9-C9A-C4A	108.63	108.32	108.45
C9A-C4A-C4Aa	106.60	106.81	106.71
C4A-C4Aa-C9Aa	106.60	106.81	106.71
C4Aa-C9Aa-N9	108.63	108.32	108.45
C9A-C1-C2	117.33	118.02	117.66
C1-C2-C3	121.61	121.28	121.33
C2-C3-C4	120.93	120.70	120.72
C3-C4-C4A	118.85	119.11	119.21
C4-C4A-C9A	119.43	119.57	119.20
C4A-C9A-C1	121.85	121.31	121.88
C1a-C9Aa-C4Aa	121.85	121.31	121.88
C9Aa-C4Aa-C4a	119.43	119.57	119.21
C4Aa-C4a-C3a	118.85	119.11	119.21
C4a-C3a-C2a	120.93	120.70	120.72
C3a-C2a-C1a	121.61	121.28	121.33
C2a-C1a-C9Aa	117.33	118.02	117.66

**Table 2:** Calculated Bond Angles using DFT compared to Measured Bond Angles from X-ray diffraction data

In the pyrrole ring, two angles, N9-C9A-C4A and C4Aa-C9Aa-N9, are underestimated in the calculation using both basis sets though the deviation is more (0.31 Å) when the 3-21G basis set is used (Table 2). The angles C9A-C4A-C4Aa and C4a-C4Aa-

C9Aa are overestimated by the using the basis sets though here also the 3-21G gives a higher deviation of 0.21 Å (Table 2). The angle at the nitrogen atom, 109.53 Å is also overestimated using both basis sets though as usual the 3-21G basis set gives a higher overestimation, 0.2 Å. This is expected as the 3-21G is a lower level of theory.

In the arene rings, the angles furthest from the nitrogen, C4 and C4a are better estimated by the DFT with a deviation (0.26 Å using 3-21G and 0.36 Å using 6-31Gd basis sets). This is as expected since the influence of the nitrogen is minimal here.

### Natural Bond Orbital (NBO) Analysis

The two bonds being shared by the pyrrole ring and the arene rings, C4A-C9A and C4Aa-C9Aa, have an index of 2 (double bond) and are the same length, 1.4145 (15) Å (SC x-ray data) or 1.4263 Å (DFT) though they are longer than the other four double bonds in the arene rings. This is expected since bond lengths in pyrrole rings are usually longer.

The NBO from these bonds are composed of approximately 50% from each carbon hybrid. One bond is composed of  $sp^{2.33}$  for the carbon furthest from the N and  $sp^{1.95}$  for the other carbon hybrid. The second bond is 100% p in character. As expected, the polarization coefficient for the carbon nearest the nitrogen atom is higher than the other carbon due to the influence of the nitrogen hybrid.

The NBO from the N-C bond is composed of 38% carbon hybrid and 62% nitrogen hybrid. The polarization coefficients are 0.7870 for nitrogen and 0.6169 for carbon implying the NBO is more polarized towards the nitrogen than the carbon. The carbon hybrid orbital is composed of  $sp^{2.79}$  while that of the nitrogen is  $sp^{1.84}$ .

The NBO of the C-H bonds are composed mainly of the carbon hybrid  $sp^x$  ( $2.27 < x < 2.32$ ). The NBO is more polarized towards the carbon.

For the N - H bond also, the NBO is more polarized towards the nitrogen though to a higher degree than in it is towards the carbon in the C-H NBOs. The nitrogen hybrid is  $sp^{2.39}$  and contributes 72% to the NBO.

The Carbazole molecule is more polarizable in a protic solvent (Ethanol:Water (1:1) mixture) than in an aprotic solvent (acetone) (Table 3).

Molecular Specie	Dipole Moment (debye)
Carbazole in Ground State (in vacuum)	1.4466
Carbazole in Ethanol:Water (1:1) solvent	1.5054
Carbazole in Acetone	1.4853

Table 3: Dipole Moments of Carbazole molecule in different solvents [14,45]

Supporting Information S1 gives data on the Natural Bond Orbitals.

### Analysis of Vibrational Spectrum (Infra-Red Spectrum)

IR-Spectroscopy is an efficient method to determine the geometric structure of the molecules and has been used widely in studying the structural consequences using the vibrations generated thereof [46].

### Degrees of Freedom and Modes of Vibrational Motion

Degree of freedom is the number of variables required to describe the motion of a particle completely. For non-linear molecules, all rotational motions can be described in terms of rotations around 3 axes, the rotational degree of freedom is 3 and the remaining  $3N-6$  degrees of freedom constitute vibrational motion where N is the number of atoms [47].

The number of atoms in Carbazole is 22. The degrees of freedom which constitute vibrational motion is therefore 60.

The number of the different types of vibrational motion or modes in the molecule are constituted as 21 Stretching modes, 20 Bending modes and 19 Torsion modes. Out of these there are 24 CH modes.

### Potential Energy Distribution (PED) analysis

The PED analysis is more accurate than the visualization of an atom movement to interpret a theoretical vibrational spectrum of a molecule. It also quantitatively describes the contribution to movement of a given group of atoms in a normal mode [43]. The Total Energy Distribution, TED, data generated from PED is used in discussing the IR spectrum of the compound.

The highest peak at  $759.87\text{ cm}^{-1}$  is assigned to the stretching of the C2 - H2 bond and the bending of the H3 - C3 - C4 angle. This peak is shown calculated at  $756.69\text{ cm}^{-1}$  (Figure 2).

The C - H and C - C stretching vibrations of Carbazole are predicted at  $1516.17\text{ cm}^{-1}$  (C2a - H2a),  $1367.21\text{ cm}^{-1}$  (C3 - H3),  $1257.58\text{ cm}^{-1}$  (C1 - H1), and  $771.17\text{ cm}^{-1}$  (C3a - H3a) for the C - H bonds and  $1014.64\text{ cm}^{-1}$  (C2 - C1) for the C - C bond (Figure 2). These were observed experimentally at  $1492.22\text{ cm}^{-1}$ ,  $1335.43\text{ cm}^{-1}$ ,  $1233.46\text{ cm}^{-1}$ ,  $756.69\text{ cm}^{-1}$  and  $1010\text{ cm}^{-1}$  respectively (Figure 3). These

stretching vibrations are predicted to be pure nodes. The N - C stretching vibration is also predicted to be a pure node at  $1250.38 \text{ cm}^{-1}$  (N9 - C9A) and this was observed at  $1233.46 \text{ cm}^{-1}$ .

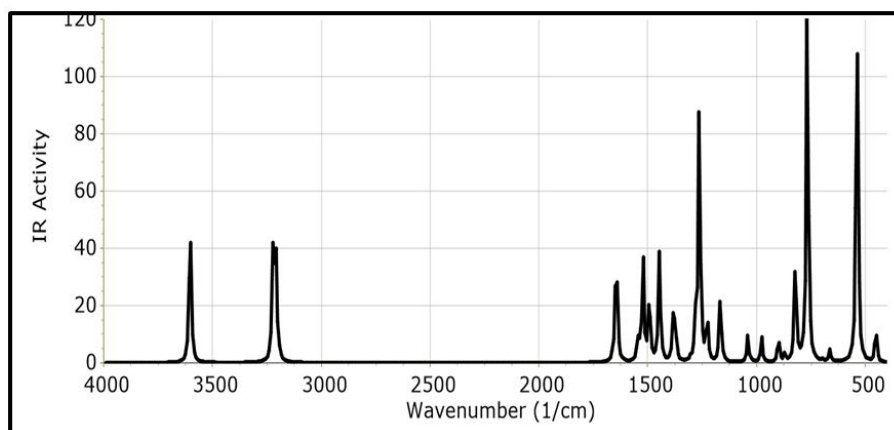


Figure 2: Calculated Infra-red spectrum of Carbazole from single crystal x-ray diffraction data

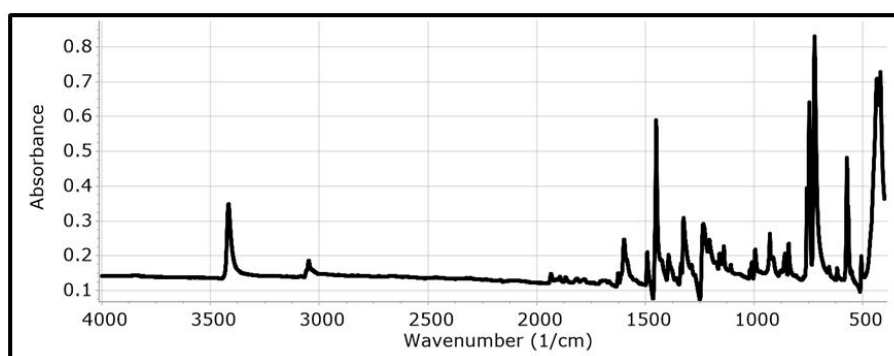


Figure 3: Experimentally determined Infra-red spectrum of Carbazole

Bending pure modes are predicted at  $1058.03 \text{ cm}^{-1}$  (H2 - C2 - C3),  $892.65 \text{ cm}^{-1}$  (C2 - C1 - C9A),  $609.81 \text{ cm}^{-1}$  (H9 - N9 - C9Aa),  $580.53 \text{ cm}^{-1}$  (H4 - C4 - C4A) and  $463.15 \text{ cm}^{-1}$  (C4Aa - C4a - C3a) (Figure 2). These were observed at  $1019.42 \text{ cm}^{-1}$ ,  $857.44 \text{ cm}^{-1}$ ,  $573.41 \text{ cm}^{-1}$  and  $551.26 \text{ cm}^{-1}$  respectively (Figure 3).

The PED analysis showed that the C - C and N - C stretching, bending and torsion vibrations are mixed with other vibrations and with themselves. An example is the prediction of a mode at  $1610.62 \text{ cm}^{-1}$  for the stretching of C4a - C4Aa mixed with the stretching of C4 - C4A which was observed at  $1598.3 \text{ cm}^{-1}$ . Another example is the mode predicted at  $1377.01 \text{ cm}^{-1}$  for the stretching of N9 - C9A and the bending of N9 - C9A - C1 which was observed at  $1335.43 \text{ cm}^{-1}$ .

Supporting Information S2 gives a comprehensive table of these modes.

### Ultra Violet Spectrum

The Ultraviolet region falls in the wavelength range 190 nm - 380 nm of the electromagnetic spectrum while the visible region falls between 380 nm and 750 nm. The Ultra-Violet spectrum of a solution of Carbazole dissolved in a solvent mix of Ethanol:Water (1:1 by volume) was determined experimentally and by computational methods using the Gaussian 09 package [14]. The major

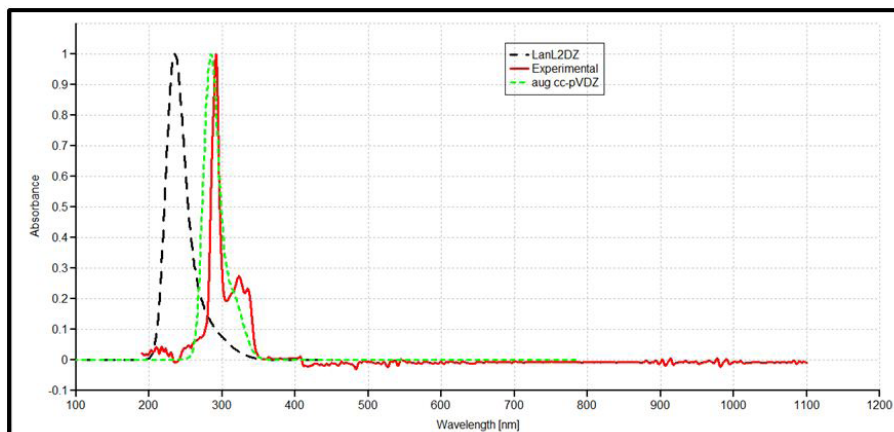


Figure 4: Experimentally determined and Calculated UV Normalized Spectra of Carbazole in Ethanol:Water mixed solvent

absorption peaks of Carbazole are in the UV range hence the powder is not coloured [48]. The experimental UV spectrum of Carbazole gives the highest absorbance at 291 nm with minor peaks at 323 nm and 333 nm (Figure 4).

Density Functional Theory (DFT) calculations using TD-SCF at B3LYP level of theory using two basis sets was performed. The cc-pVDZ basis set augmented with diffuse functions gives one major peak at 284 nm and a shoulder at 314.8 nm while the LanL2DZ basis set gives a major peak at 235.1 nm [36-40].

The difference in the wavelengths for the peak absorptions may be attributed to the approximations made by the TD-SCF models; the aug-cc-pVDZ basis set gives a better approximation of the UV spectrum since it uses a correlation consistent basis set which is augmented with diffuse functions and is appropriate for excited states of electrons. The LanL2DZ basis set on the other hand is an all electron valence double zeta basis set.

## Electronic Transitions

To simplify the analysis of DFT computed data, the structure of the carbazole drawn using the OLEX 2 and ORTEP<sup>49</sup> package was divided into the arene groups and the pyrrole group (Figure 5)[13].

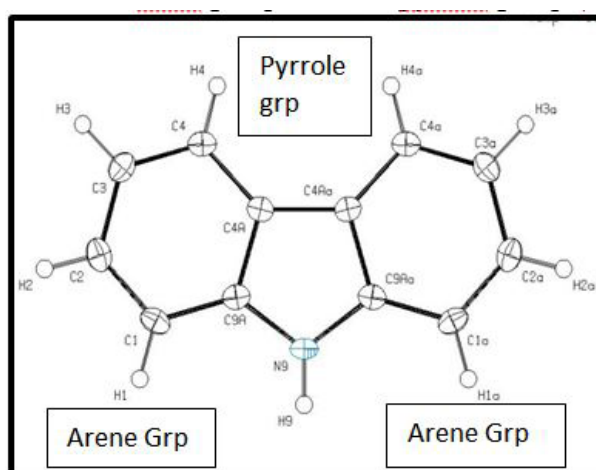


Figure 5: Labeled Carbazole showing 'groups' [49]

Electronic Transitions of the Carbazole molecule in the ground state were analysed (Table 4). The intensities have also been assessed based on oscillator strengths ( $f$ ) in the solvents for the ultraviolet induced electronic transitions.

Excitation Energy (eV)	Excitation Wavelength (nm)	Oscillator strength ( $f$ )	Major contributing orbitals	Minor Contributing orbitals
4.3648 eV	284.05	0.2135	H-1→LUMO (81.6%)	HOMO → L+1 (14.66%), H-2 → LUMO (1.47%), HOMO → L+7 (0.88%)
3.9379 eV	314.85	0.0422	HOMO→LUMO (93.7%)	H-1 → L+1 (4.95%), H-3 → L+5 (0.43%), H-1 → L+7 (0.40%)
4.9562 eV	250.16	0.0007	HOMO→L+2 (96.1%)	HOMO → L+4 (1.16%), HOMO → L+6 (1.13%), H-2 → L+3 (0.45%)

Table 4: Calculated Absorptions and the transitions responsible for Carbazole molecule in Ground State

Using the GaussSum package, the highest peak in the UV spectrum is at 284 nm is due to the absorption for the transition from the orbital one orbital lower than the Highest Occupied Molecular Orbital, HOMO, (H-1) to the Lowest Unoccupied Molecular Orbital, LUMO (82%) with a minor contribution from the HOMO to L+1 (14.66%), H-2 to LUMO (1.47%) and HOMO to L+7 (0.88%). This is attributed to  $\pi$  Arene  $\rightarrow$   $\pi^*$  Arene transition. Other absorption wavelengths and the transitions responsible for them are given [44] (Table 4).

## Frontier Molecular Orbitals

Frontier Molecular Orbitals (FMO) theory is one of the best theories to explain the chemical stability of a molecule. Highest Occupied Molecular Orbital (HOMO) and Lowest Unoccupied Molecular Orbital (LUMO) are important orbitals of FMOs.

The HOMO energy is related to the ability of the molecule in releasing an electron, whereas the LUMO energy gives that of gaining an electron.

The Frontier Orbital Gap, FOG, the difference between the LUMO and the HOMO, is an important index for the chemical reactivity and kinetic stability of a molecule. It also measures the resistance to change in electron distribution in a molecule [50].

A molecule with a low frontier orbital gap is more polarizable and will exhibit a significant degree of intramolecular charge-transfer from the electron donor section to the electron acceptor section [51].

The Frontier Molecular Orbitals of the molecule in gas and when dissolved in a solvent system were assessed and it showed that when the molecule is dissolved in the solvent system of Ethanol:water (1:1 by volume), the molecule is more polarizable due to the dissolution.

### Energy Levels of Molecular Orbitals

Energies in electron Volts of the various molecular orbitals of the molecule in vacuum, when dissolved in a protic solvent, (solvent mix of Ethanol:Water [1:1 by volume]) and when dissolved in an aprotic solvent, acetone, with the solution exposed to ultraviolet waves were also assessed. GaussSum was used to determine the percentage contribution of the various 'groups' in the molecule [44] (Table 5,6 and 7). [Carbazole is soluble in ethanol and acetone] [52].

Molecular Orbital		Energy eV	% Arenes	% Pyrrole
Level	Label			
47	L+2	1.00	88	12
46	L+1	0.26	100	0
45	LUMO	-0.62	99	1
44	HOMO	-5.52	74	26
43	H-1	-5.84	100	0
42	H-2	-6.92	100	0
41	H-3	-7.65	99	1
40	H-4	-8.94	72	28

**Table 5:** Contributions of groups to Molecular Orbitals of Carbazole in Ground State in gas

The band gap, given as the difference between the HOMO and the LUMO, is 4.90 eV. The LUMO is made up mainly from the arene groups, with the pyrrole group contributing only 1%. The HOMO is made up of 74% contribution from the arene groups with the pyrrole group contributing the remaining 26%.

Molecular Orbital		Energy eV	% Arenes	% Pyrrole
Level	Label			
47	L+2	-0.22	56	44
46	L+1	-0.36	99	1
45	LUMO	-1.27	100	0
44	HOMO	-5.88	76	24
43	H-1	-6.19	99	1
42	H-2	-7.23	99	1
41	H-3	-7.97	99	1
40	H-4	-9.24	72	28

**Table 6:** Contributions of groups to Molecular Orbitals Carbazole in Ethanol:Water (1:1) mixed solvent exposed to UV [14,44]

When the molecule in the mixed solvent is irradiated with UV in the spectrophotometer, the band gap is reduced to 4.61 eV. The contributions by the various groups however did not change much; the LUMO is made up solely from the arene groups (100%),

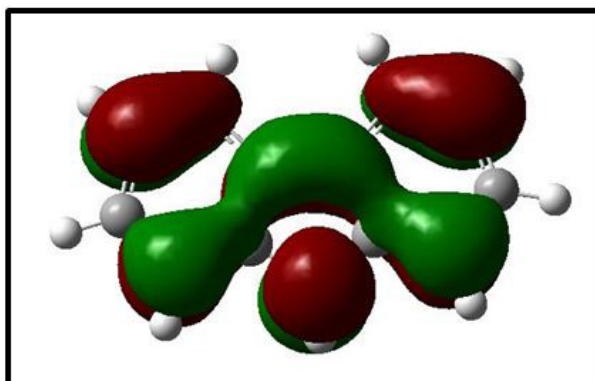


**Figure 6:** Highest Occupied Molecular Orbital HOMO of Excited Carbazole molecule in Ethanol:Water solvent; Energy = -5.88eV

and the pyrrole group contributes 24% to the HOMO while the arene groups contribute 76% to the HOMO similar to that of the molecule in the ground state (Figure 6,7).

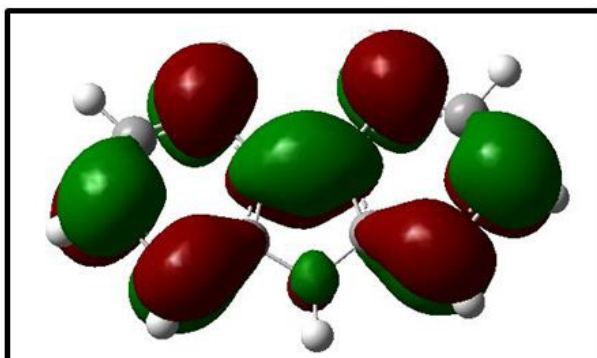


**Figure 7:** Lowest Unoccupied Molecular Orbital of Excited Carbazole molecule in Ethanol:Water solvent;  $E = -1.27\text{eV}$

When the molecule in acetone is irradiated with UV in the spectrophotometer, however, the band gap is increased to 5.01 eV. The contributions by the various groups however did not change much; the LUMO made up solely from the arene groups (100%). The arene groups also contribute 72% to the HOMO while the pyrrole group contribute only 28% to the HOMO (Table 7).

Molecular Orbital		Energy eV	% Arenes	% Pyrrole
Level	Label			
47	L+2	-0.4	99	1
46	L+1	-0.43	88	12
45	LUMO	-1.29	100	0
44	HOMO	-6.3	72	28
43	H-1	-6.36	100	0
42	H-2	-7.21	99	1
41	H-3	-7.89	98	2
40	H-4	-8.96	64	36

**Table 7:** Contributions of groups to Molecular Orbitals of Carbazole in Acetone exposed to UV [14,44]

## Powder Diffraction

Powder diffraction is a scientific technique using X-ray, neutron, or electron diffraction on powder or microcrystalline samples for structural characterization of materials. It is a non-destructive procedure [53].

About 95% of all solid materials can be described as crystalline. When X-rays interact with a crystalline substance (Phase), one gets a diffraction pattern.

This procedure is based on the assumption that ideally, every possible crystalline orientation is represented equally in a powdered sample. The resulting orientational averaging causes the three-dimensional reciprocal space that is studied in single crystal diffraction to be projected onto a single dimension.

Each compound, regarded as a phase, gives a distinct characteristic diffractogram when analysed.

The position and intensity of peaks in a diffraction pattern are determined by the crystal structure. The scattering of X-rays from atoms produces a diffraction pattern, which contains information about the atomic arrangement within the crystal [54].

The X-ray diffraction pattern of a pure substance is, therefore, like a fingerprint of the substance. The powder diffraction method is thus ideally suited for characterization and identification of polycrystalline phases

Each substance is characterized by its three strongest lines ( $d_1$ ,  $d_2$ ,  $d_3$ ). The values of  $d_1$ -  $d_3$  are usually sufficient to characterize the pattern of an unknown and enable the corresponding pattern in a database such as the Powder Diffraction File to be located [55-57].

Any one diffraction pattern is characterised by a set of line positions  $2\theta$  and a set of relative intensities. Exact matching of the interplanar spacings ( $d$  values) and intensities of all peaks (or lines in the case of powder camera) between the standard and observed diffraction patterns confirms the identity of the unknown as the same as the standard material [58].

The powder diffraction pattern, diffractogram, of carbazole experimentally determined has its three major peaks at  $2\theta$  similar

to those the diffractogram simulated using single crystal data as reported by Gajda *et al.* [12](Table 8). The simulation was done using the Mercury software [59].

Experimental Carbazole PXRD		Simulated Carbazole PXRD	
2 Theta (deg)	Absorbance	2 Theta (deg)	Absorbance
9.2	1	9.3	0.9639
18.48	0.2776	20.02	1
27.84	0.2828	28.54	0.8737

**Table 8:** Highest peaks in Experimental and Simulated Carbazole PXRD

All other peaks of the diffractogram determined experimentally are also adequately close to those in the diffractogram simulated from single crystal data of Carbazole published by Gajda *et al.* (Figure 8).

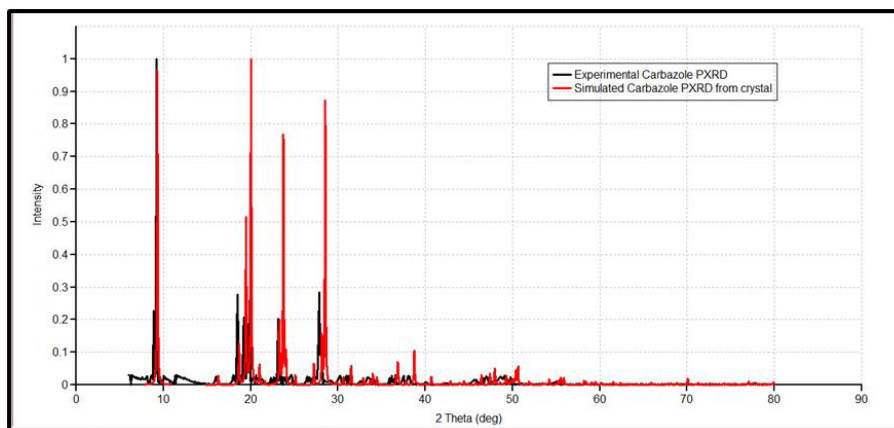


**Figure 8:** Experimentally determined and Simulated Powder X-ray Diffractograms of Carbazole

The differences in resolution were due to the scanning step size which was  $0.08^\circ$  experimentally and  $0.02^\circ$  when simulated from the single crystal structure.

The d-spacing of the six most intense peaks in the experimentally determined diffractogram vary from  $3.18535 \text{ \AA}$  to  $9.64307 \text{ \AA}$  (Table 9).

2 Theta [°]	Height [cts]	d-spacing [Å]	Rel. Int. [%]
9.1711	125,428.0	9.64307	100.00
19.7092	32,153.8	4.50449	25.64
28.0122	23,336.78	3.18535	18.61
23.227	19,537.5	3.82963	15.58
18.452	17,043.2	4.80847	13.59
19.1258	13,477.1	4.64057	10.74

**Table 9:** Six most intense peaks in Carbazole powder diffractogram

## Conclusion

Both basis sets, 3-21G and 6-31Gd, used in calculating the structural parameters of Carbazole gave good approximations though generally, the 3-21G basis set performed better. The calculated bond lengths are generally longer and the calculated angles wider than those determined experimentally.

The double bonds shared by the pyrrole ring and the arene rings are longer than those in the arene rings alone though in all cases the second bond is 100% p in character.

A third of the vibrational modes are from C-H stretching.

Bonds are more polarized towards the nitrogen atom than the carbon as expected (from their electronegativity values). The Carbazole molecule is more polarizable when dissolved in a protic solvent of Ethanol:Water (1:1) than in an aprotic solvent (acetone).

The arene group in the molecule of Carbazole contributes about 100% to its Lowest Unoccupied Molecular Orbital (LUMO) and about 75% to its Highest Occupied Molecular Orbital (HOMO). Dissolution of Carbazole in a protic solvent, Ethanol:Water mixture, reduces its Frontier Orbital Gap (FOG) by about 6% but increases by about 2.2% when it is dissolved in an aprotic solvent, acetone.

The major UV peak at 291 nm (284 nm calculated) is from the transition from HOMO-1 to the LUMO level and is due to  $\pi \rightarrow \pi^*$  transition by the arene groups.

The powder diffractogram of Carbazole has its characteristic peaks, d1, d2 and d3 at  $2\theta$  of  $9.2^\circ$ ,  $18.48^\circ$  and  $27.84^\circ$ .

## Supporting Information

S1: Natural Bond Orbitals of Carbazole

S2: Normal Vibrational Modes of bonds in Carbazole

## References

1. Zhang, FF, Gan LL, Zhou CH (2010) Synthesis, antibacterial and antifungal activities of some carbazole derivatives. *Bioorg Med Chem Lett* 20: 1881-4.
2. Nandy BC, Gupta AK, Mittal A, Vyas V (2014) Carbazole: it's biological activity. *J Biomed Pharm Res* 3: 42-8.
3. Ravichandiran P, Jegan A, Premnath D, Periasamy VS, Muthusubramanian S, et al. (2014) Synthesis, molecular docking and cytotoxicity evaluation of novel 2-(4-amino-benzosulfonyl)-5H-benzo[b]carbazole-6,11-dione derivatives as histone deacetylase (HDAC8) inhibitor. *Bioorg Chem* 53: 24-36.
4. Ravichandiran P, Premnath D, Kumar SV (2014) Design, Synthesis, Molecular Docking and Antibacterial evaluation of novel N-(6, 11-dioxo-dihydro-5H-benzo [B] carbazol-2yl) Benzamide derivatives as potent antibacterial agents. *Int J Pharm Sci* 6: 244-49.
5. Zhang Q, Jiangshan C, Yanxiang C, Lixiang W, Dongge MA, et al.(2004) Novel hole-transporting materials based on 1,4-bis(carbazolyl)benzene for organic light-emitting devices. *J Mater Chem* 14: 895-900.
6. Friend RH, Gymer RW, Holmes AB, Burroughes JH, Marks RN, et al. (1999) Electroluminescence in conjugated polymers *Nature* 397: 121-8.
7. Leutwyler S, Bösiger J (1990) Rare-Gas Solvent Clusters: Spectra, Structures, and Order-Disorder Transitions *Chem Rev* 90: 489-507.
8. Honegger E, Bombach R, Leutwyler S (1986) Intermolecular bonding and vibrations of the carbazole#B complexes (B=H<sub>2</sub>O, D<sub>2</sub>O, NH<sub>3</sub>). *J Chem Phys* 85: 1234-46.
9. Lee SY, Boo BH (1996) Molecular Structures and Vibrational Spectra of Pyrrole and Carbazole by Density Functional Theory and Conventional ab Initio Calculations. *J Phys Chem* 100: 15073-8.
10. Bree A, Zwarich R (1968) Vibrational Assignment of Carbazole from Infrared, Raman, and Fluorescence Spectra. *J Chem Phys* 49: 3344-55.
11. Menges F (2015) Spekwin32 - optical spectroscopy software.
12. Gajda K, Zarycht B, Kopk K, Daszkiewicz Z, Ejsmont K (2014) Substituent effects in nitro derivatives of carbazoles investigated by comparison of low-temperature crystallographic studies with density functional theory (DFT) calculations. *Acta Crystallogr C Struct Chem* 70: 987-91.
13. Dolomanov OV, Bourhis LJ, Gildea RJ, Howard JAK, Puschmann H (2009) Olex 2: A complete structure solution, refinement and analysis program. *J Appl Cryst* 42: 339-41.
14. Frisch MJ (2009) Gaussian 09.
15. Becke AD (1993) Density-functional thermochemistry. III. The role of exact exchange. *J Chem Phys* 98: 5648-52.
16. Binkley JS, Pople JA, Hehre WJ (1980) Self-Consistent Molecular Orbital Methods. 21. Small Split-Valence Basis Sets for First-Row Elements. *J Am Chem Soc* 102: 939-47.
17. Gordon MS, Binkley JS, Pople JA, Pietro WJ, Hehre WJ (1982) Self-Consistent Molecular Orbital Methods. 22. Small Split-Valence Basis Sets for Second-Row Elements. *J Am Chem Soc* 104: 2797-803.
18. Pietro WJ (1982) Self-Consistent Molecular Orbital Methods. 24. Supplemented small split-valence basis-sets for 2ndrow elements. *J Am Chem Soc* 104: 5039-48.
19. Dobbs KD, Hehre WJ (1987) Molecular-orbital theory of the properties of inorganic and organometallic compounds. 5. Extended basis-sets for 1st-row transition-metals. *J Comp Chem* 8: 880-93.
20. Dobbs KD, Hehre WJ (1987) Molecular-orbital theory of the properties of inorganic and organometallic compounds. 6. Extended basis-sets for 2nd-row transition-metals. *J Comp Chem* 8: 880-93.
21. Ditchfield R, Hehre WJ, Pople JA (1971) Self-Consistent Molecular Orbital Methods. 9. Extended Gaussian-type basis for molecular-orbital studies of organic molecules *J Chem Phys* 54: 724.
22. Hehre WJ, Ditchfield R, Pople JA (1972) Self-Consistent Molecular Orbital Methods. 12. Further extensions of Gaussian-type basis sets for use in molecularorbital studies of organic-molecules. *J Chem Phys* 56: 2257.
23. Hariharan PC, Pople JA (1973) Influence of polarization functions on molecularorbital hydrogenation energies. *Theoretica Chimica acta* 28: 213-22.
24. Hariharan, PC, Pople JA (1974) Accuracy of AH equilibrium geometries by single determinant molecular-orbital theory. *Mol Phys* 27: 209-14.
25. Gordon MS (1980) The isomers of silacyclopropane *Chem Phys Lett* 76: 163-8.
26. Francl MM (1982) Self-Consistent Molecular Orbital Methods. 23. A polarization-type basis set for 2nd-row elements. *J Chem Phys* 77: 3654-65.
27. Binning RC, Curtiss LA (1990) Compact contracted basis-sets for 3rd-row atoms - GA-KR. *J. Comp. Chem.* 11: 1206-16.
28. Blaudeau JP, McGrath MP, Curtiss LA, Radom L (1997) Extension of Gaussian-2 (G2) theory to molecules containing third-row atoms K and Ca. *J Chem Phys* 107: 5016-21.
29. Rassolov VA, Pople JA, Ratner MA, Windus TL (1998) 6-31G\* basis set for atoms K through Zn. *J Chem Phys* 109: 1223-9.
30. Rassolov VA, Ratner MA, Pople JA, Redfern PC & Curtiss LA (2001) 6-31G\* Basis Set for Third-Row Atoms. *J Comp Chem* 22: 976-84.
31. Petersson GA (1988) A complete basis set model chemistry. I. The total energies of closedshell atoms and hydrides of the first-row atoms. *J Chem Phys.* 89: 2193-218.

32. Petersson GA, Al-Laham MAA (1991) complete basis set model chemistry. II. Open-shell systems and the total energies of the first-row atoms. *J Chem Phys* 94: 6081-90.
33. Dunning TH, Hay PJ (1976) *Modern Theoretical Chemistry* (Schaefer-III edn) 1-28.
34. Cossi M, Rega N, Scalmani G, Barone V (2003) Energies, structures, and electronic properties of molecules in solution with the C-PCM solvation model. *J Comp Chem* 24: 669-81.
35. Barone V, Cossi M (1998) Quantum calculation of molecular energies and energy gradients in solution by a conductor solvent model. *J Phys Chem* 102: 1995-2001.
36. Dunning TH (1989) Gaussian basis sets for use in correlated molecular calculations. I. The atoms boron through neon and hydrogen. *J Chem Phys* 90: 1007-23.
37. Woon DE, Dunning TH (1993) Gaussian-basis sets for use in correlated molecular calculations. 3. The atoms aluminum through argon. *J Chem Phys* 98: 1358-71.
38. Wilson AK, Mourik TV, Dunning TH (1996) Gaussian Basis Sets for use in Correlated Molecular Calculations. VI. Sextuple zeta correlation consistent basis sets for boron through neon. *J Mol Struct* 388: 339-49.
39. Kendall RA, Dunning TH, Harrison RJ (1992) Electron affinities of the first-row atoms revisited. Systematic basis sets and wave functions. *J Chem Phys* 96: 6796-806.
40. Peterson KA, Woon DE, Dunning TH (1994) Benchmark calculations with correlated molecular wave functions. IV. The classical barrier height of the  $H+H_2 \rightarrow H_2+H$  reaction. *J chem phys* 100: 7410.
41. Davidson ER (1996) Comment on "Comment on Dunning's correlation-consistent basis sets. *Chem. Phys. Lett.* 260: 514-18.
42. Jamróz MH (2015) *Vibrational Energy Distribution Analysis (VEDA)* 4.
43. Jamróz MH (2013) Vibrational energy distribution analysis (VEDA): scopes and limitations. *Spectrochim Acta A Mol Biomol Spectrosc* 114: 220-30.
44. O'Boyle NM, Tenderholt AL, Langner KM (2008) cclib: a library for package-independent computational chemistry algorithms. *J Comput Chem* 29: 839-45.
45. Frisch AE (2009) *GaussView 5.0*. 1-102.
46. Thanigaimani K, Khalib NC, Temel E, Arshad S, Razak IA (2015) New supramolecular cocrystal of 2-amino-5-chloropyridine with 3-methylbenzoic acids: Syntheses, structural characterization, Hirshfeld surfaces and quantum chemical investigations. *J Mol Struct* 1099: 246-56.
47. Banks R, Chu C, Sinha G (2010) *Vibrational Modes*.
48. (2015) *SpectraSchool - Infra Red Spectroscopy*.
49. Spek AL (2009) Structure validation in chemical crystallography. *Acta Crystallogr D Biol Crystallogr.* 65: 148-55.
50. Manimekalai A, Vijayalakshmi N (2015) Computational and Spectral studies of 6-phenylazo-3-(p-tolyl)-2H-chromen-2-one. *Spectrochim. Acta - Part A Mol Biomol Spectrosc* 136: 388-96
51. Li L, Wu C, Wang ZI, Zhao L, Li Z, et al. (2015) Density functional theory (DFf) and natural bond orbital (NBO) study (I) of vibrational spectra and intramolecular hydrogen bond interaction of CroaMm: L-ornithine-L-aspartate. *Spectrochim. Acta Part A Mol. Biomol Spectrosc* 22: 338-46
52. Merck Index (2016) Carbazole.
53. Wikipedia contributors (2016) Powder Diffraction.
54. Speakman SA (1999) *Basics of X-Ray Powder Diffraction*.
55. *Basics of X-ray Diffraction*. in (Scintag Inc., 1999).
56. Moeck P (2014) *X-Ray Diffraction (XRD) Powder*.
57. Hanawalt JD, Rinn HW(1986) *Identification of Crystalline Materials - Classification and use of X-ray Diffraction Patterns*. *J Powder Diffr* 1:1-5.
58. Ahmad N, Norhayati Ahmad (2011) *Teaching & Learning Site*.
59. Macrae CF, Bruno IJ, Chisholm JA, Edgington PR, McCabe P, et al. (2008)Mercury CSD 2.0 - new features for the visualization and investigation of crystal structures. *J Appl Crystallogr* 41: 466-70.